

## Journal Publication

# The role of the gas/plasma plume and self-focusing in a gas-filled capillary discharge waveguide for high-power laser-plasma applications

Ciocarlan, C. (University of Strathclyde and Horia Hulubei National Institute of Physics and Nuclear Engineering) *et al*

24 September 2013



The EuCARD-2 Enhanced European Coordination for Accelerator Research & Development project is co-funded by the partners and the European Commission under Capacities 7th Framework Programme, Grant Agreement 312453.

This work is part of EuCARD-2 Work Package **13: Novel Acceleration Techniques (ANAC2)**.

The electronic version of this EuCARD-2 Publication is available via the EuCARD-2 web site <http://eucard2.web.cern.ch/> or on the CERN Document Server at the following URL: <http://cds.cern.ch/search?p=CERN-ACC-2013-0316>

**The role of the gas/plasma plume and self-focusing in a gas-filled capillary discharge waveguide for high-power laser-plasma applications**

C. Ciocarlan, S. M. Wiggins, M. R. Islam, B. Ersfeld, S. Abuazoum, R. Wilson, C. Aniculaesei, G. H. Welsh, G. Vieux, and D. A. Jaroszynski


Citation: *Physics of Plasmas* (1994-present) **20**, 093108 (2013); doi: 10.1063/1.4822333


View online: <http://dx.doi.org/10.1063/1.4822333>

View Table of Contents: <http://scitation.aip.org/content/aip/journal/pop/20/9?ver=pdfcov>


Published by the [AIP Publishing](#)

---



 Vacuum Solutions from a Single Source

- Turbopumps
- Backing pumps
- Leak detectors
- Measurement and analysis equipment
- Chambers and components

**PFEIFFER**  **VACUUM**

# The role of the gas/plasma plume and self-focusing in a gas-filled capillary discharge waveguide for high-power laser-plasma applications

C. Ciocarlan,<sup>1,2</sup> S. M. Wiggins,<sup>1,a)</sup> M. R. Islam,<sup>1</sup> B. Ersfeld,<sup>1</sup> S. Abuazoum,<sup>1</sup> R. Wilson,<sup>1</sup>  
 C. Aniculaesei,<sup>1</sup> G. H. Welsh,<sup>1</sup> G. Vieux,<sup>1</sup> and D. A. Jaroszynski<sup>1,b)</sup>

<sup>1</sup>Department of Physics, Scottish Universities Physics Alliance, University of Strathclyde, Glasgow G4 0NG, United Kingdom

<sup>2</sup>Department of Nuclear Physics, Horia Hulubei National Institute of Physics and Nuclear Engineering, 76900 Bucharest-Magurele, Romania

(Received 15 May 2013; accepted 4 September 2013; published online 24 September 2013)

The role of the gas/plasma plume at the entrance of a gas-filled capillary discharge plasma waveguide in increasing the laser intensity has been investigated. Distinction is made between neutral gas and hot plasma plumes that, respectively, develop before and after discharge breakdown. Time-averaged measurements show that the on-axis plasma density of a fully expanded plasma plume over this region is similar to that inside the waveguide. Above the critical power, relativistic and ponderomotive self-focusing lead to an increase in the intensity, which can be nearly a factor of 2 compared with the case without a plume. When used as a laser plasma wakefield accelerator, the enhancement of intensity can lead to prompt electron injection very close to the entrance of the waveguide. Self-focusing occurs within two Rayleigh lengths of the waveguide entrance plane in the region, where the laser beam is converging. Analytical theory and numerical simulations show that, for a density of  $3.0 \times 10^{18} \text{ cm}^{-3}$ , the peak normalized laser vector potential,  $a_0$ , increases from 1.0 to 1.85 close to the entrance plane of the capillary compared with  $a_0 = 1.41$  when the plume is neglected. © 2013 AIP Publishing LLC. [<http://dx.doi.org/10.1063/1.4822333>]

## I. INTRODUCTION

The gas-filled capillary discharge waveguide (CDW) is a useful medium for investigating high-power laser-plasma interactions over extended lengths because guiding can increase the interaction length to many Rayleigh lengths.<sup>1</sup> Major applications of these waveguides include the laser-plasma wakefield accelerator (LWFA),<sup>2–7</sup> where terawatt-scale femtosecond laser pulses are used to generate MeV,<sup>8–10</sup> and GeV<sup>11</sup> electron beams over typical lengths of 30–40 mm, and the plasma-based Raman amplifier,<sup>12,13</sup> where two counter-propagating laser pulses in a CDW allow resonant transfer of energy from a “pump” laser pulse to a “probe” pulse. In both of these applications, there is an increasing trend towards using very high incident laser powers, where relativistic effects can become important.<sup>14,15</sup>

The gas-filled CDW is formed when a potential difference of 10–20 keV is applied between two electrodes located at either end of a capillary to initiate a discharge in readily ionized gas such as hydrogen. The gas is pre-injected into the capillary and underdense plasma is formed via avalanche breakdown and collisional ionization.<sup>16</sup> Thermal conduction to the capillary walls results in a high on-axis plasma temperature and a temperature gradient between the axis and the wall. In equilibrium, the pressure across the capillary is uniform, which results in a parabolic radial density distribution and a refractive index profile suitable for waveguiding.

For a low-intensity laser pulse propagating in the channel, diffraction can be exactly compensated by the focusing

effect of the plasma lens and the laser pulse can be transported over several centimetres with excellent mode structure and little energy loss for a matched spot size.<sup>1,17</sup> Laser pulse propagation at very high intensity is modified significantly by the intensity-dependent refractive index due to relativistic effects,<sup>18</sup> and ponderomotive focusing,<sup>19</sup> which are highly nonlinear. LWFAs typically operate in the so-called bubble regime<sup>20</sup> characterized by a normalized laser vector potential  $a_0 = eA_0/m_e c > 1$ , where  $A_0$  is the vector potential,  $e$  and  $m_e$  are the charge and mass of the electron, respectively, and  $c$  is the speed of light in vacuum. Relativistic self-focusing overcomes vacuum diffraction when the power  $P_0$  exceeds a critical power,  $P_c = 17.4(\omega_0/\omega_p)^2$  [GW], where  $\omega_0$  and  $\omega_p$  are the laser and plasma frequencies, respectively. For lower power, it increases the effective Rayleigh length by a factor of  $(1 - P_0/P_c)^{-1/2}$ .<sup>21</sup> The Rayleigh length in vacuum is  $Z_R = \pi w_0^2/\lambda$ , where  $w_0$  is the  $(1/e^2)$  radius of the laser beam and  $\lambda$  its wavelength. Ponderomotive self-focusing occurs when the laser pulse duration exceeds a plasma period, so that the rear of the pulse propagates in a density channel formed by the ponderomotive pressure of the pulse front. Both processes lead to an increase in  $a_0$ , which enables strong density wake formation, electron injection, and subsequent acceleration.<sup>22</sup> Non-linear self-focusing along with diffraction and plasma guiding determine the laser pulse evolution in the CDW and the relative strengths of these processes are particularly important in the entrance region of the CDW because the laser focal plane typically coincides with the capillary entrance plane.

To fully describe the laser pulse evolution, the entrance region outside the capillary must be included in any study, which forms the topic of this paper. The plume regions,

<sup>a)</sup>Electronic mail: mark.wiggins@strath.ac.uk

<sup>b)</sup>Electronic mail: d.a.jaroszynski@strath.ac.uk

which in the case of the CDW are the regions beyond the capillary itself, are well known for material processing applications using plasma jets<sup>23</sup> or plasma guns,<sup>24</sup> but have been neglected in previous laser-plasma studies.<sup>9,25</sup> A gas-filled CDW plume has two distinct components arising from initial gas pre-injection and later discharge breakdown, i.e., there is an expanding neutral gas plume followed by an expanding plasma plume. Here, we show that the density of the gas/plasma plume is sufficiently high for laser self-focusing to occur at a significant distance in front of the entrance of the CDW. The vacuum laser focus is chosen to coincide with the entrance plane. Numerical and analytical methods are used to determine the self-focusing in the plume region and this is compared with laser evolution when the plume is neglected.

## II. CAPILLARY GEOMETRY

The schematic of our CDW system is shown in Fig. 1(a). The alumina capillary under investigation here is manufactured by femtosecond laser micromachining,<sup>26</sup> and has a length of 40 mm and diameter of 300  $\mu\text{m}$ . Gas inlets, with 0.2 mm  $\times$  0.8 mm rectangular apertures, are located 10 mm from each end of the capillary. Injection of hydrogen gas is controlled by a pulsed solenoid valve that is open for a duration of 200 ms. A high voltage electrical pulse (20 kV peak

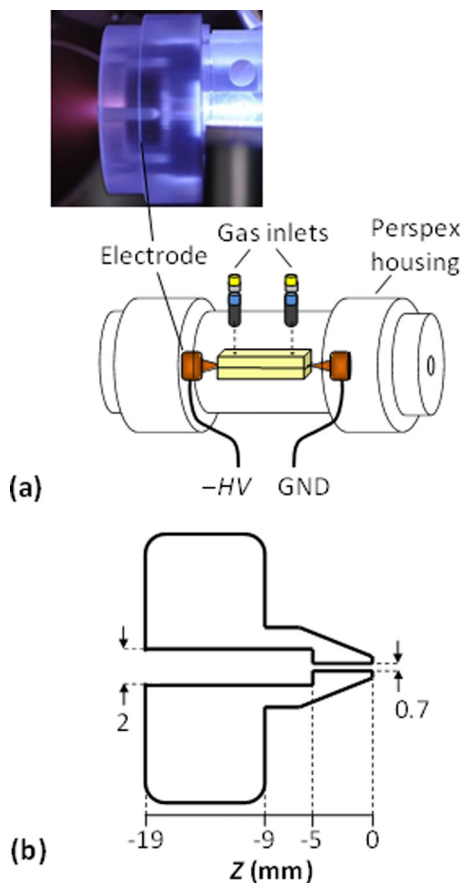


FIG. 1. (a) Schematic of the gas-filled capillary discharge plasma waveguide setup. A laser pulse enters at either or both ends. Inset: a photograph of one end of a sapphire CDW showing emission from the plasma plume exiting the electrode aperture on the left hand side. (b) Cross-section of the copper electrodes, where all units are in mm. Zero on the Z-axis coincides with the capillary entrance plane.

voltage, 900 ns full-width duration at half-maximum)<sup>27</sup> is applied 100  $\mu\text{s}$  after valve closure to initiate breakdown. The copper electrode geometry [Fig. 1(b)] shows the on-axis aperture extending from the capillary edge with a diameter of 700  $\mu\text{m}$  and widening to 2 mm at a distance of  $-5$  mm (negative distances along the laser propagation axis refer to the region outside the capillary). The high-power laser pulse is usually synchronized with the plasma current pulse on a sub-microsecond timescale. Therefore, the laser initially encounters the neutral gas plume far from the entrance plane and then, closer to the entrance, the expanding hot plasma plume that has a typical temperature of  $\approx 5$  eV.<sup>16</sup> The precise rate of plasma expansion (with a velocity of  $\sim 10^4$ – $10^5$  m/s)<sup>28,29</sup> depends on discharge characteristics and is discussed further in Sec. IV. In regions, where the intensity is greater than  $10^{14}$  W/cm<sup>2</sup> non pre-ionized gas is ionized by the intense laser field.

The plume of gas/plasma extends beyond the Perspex housing and is clearly visible to the naked eye, as shown in Fig. 1(a). However, the main region of interest is in the vicinity of the entrance plane, where the laser beam is converging. The expected focusing system in vacuum of a typical high-power laser used in LWFA experiments<sup>7,30</sup> utilizes a large  $F$ /number focusing element ( $F/16$ ) to focus the beam of wavelength  $\lambda = 800$  nm to a  $(1/e^2)$  radius  $w_0 = 20$   $\mu\text{m}$  at the entrance of the CDW, which would give an intensity of  $2.2 \times 10^{18}$  W/cm<sup>2</sup> and  $a_0 = 1.0$  at the focus in vacuum. However, in the case, where a gas/plasma plume exists in this laser focusing region, significant self-focusing enhances the rate of focusing. For our conditions, this occurs when  $a_0$  reaches a value of  $\approx 0.5$ , at  $Z = -3$  mm. This is equivalent to approximately  $-2Z_R$ , where  $Z_R = 1.6$  mm, and defines the region where laser self-focusing is important.

## III. PLUME SIMULATIONS

### A. Steady-state neutral gas flow

As a first step into gaining insight into the structure of our capillary plume, we have modelled the neutral gas density distribution under steady-state conditions using the 2D FLUENT fluid code.<sup>31</sup> Simulations have been carried out for two cases: one including the electrode geometry and the other without it, to illustrate the influence of the geometry. As shown in Fig. 2, for the steady-state case, the hydrogen molecular density between the inlets is  $3.6 \times 10^{18}$  cm<sup>-3</sup>, reducing to  $1.1 \times 10^{18}$  cm<sup>-3</sup> at the entrance (for a backing pressure of 150 mbar), when the valve is open. Upon valve closure, when the pressure reaches equilibrium, the on-axis electron plasma density is uniform when the gas is ionized along the entire capillary and  $n_e$  is estimated to be  $2.9 \times 10^{18}$  cm<sup>-3</sup> (from Ref. 32). The electrode geometry has a significant effect on the gas density profile in these simulations. In the absence of the electrodes [upper contour map of Fig. 2(a)], the gas density would decay rapidly with distance beyond the capillary entrance plane and the density at  $Z = -3$  mm is negligible ( $< 10^{17}$  cm<sup>-3</sup>). The presence of the electrodes leads to confinement of the gas [lower contour map of Fig. 2(a)], thus maintaining a relatively high density with a rapid fall-off only beyond the extent of the electrodes.

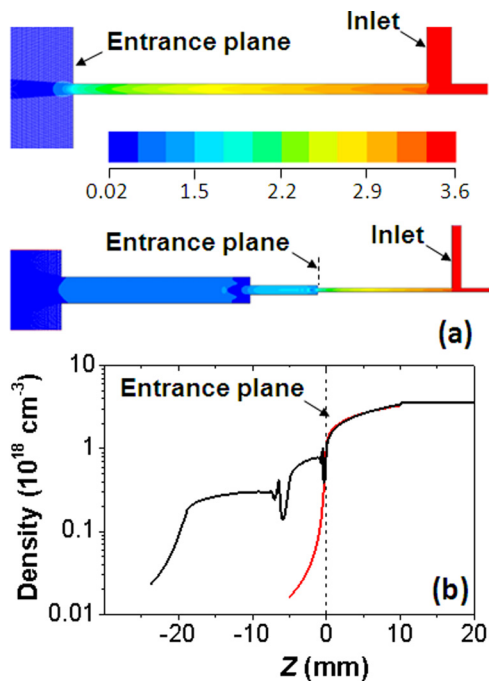


FIG. 2. Simulations of the gas density for a backing pressure of 150 mbar showing (a) contour maps in the region of the entrance plane without (upper) and with (lower) inclusion of the electrode geometry, where the gas density is given in units of  $10^{18} \text{ cm}^{-3}$ , and (b) the respective on-axis longitudinal density profiles with (black) and without (red) electrodes.

In this case,  $n_e$  is estimated to be  $\approx 0.7 \times 10^{18} \text{ cm}^{-3}$  at  $Z = -3 \text{ mm}$ .

### B. Laser self-focusing in a plasma plume

The extent of self-focusing in the plume region, assuming it is wholly comprised of plasma, has been calculated analytically and compared with simulations using the 3D axisymmetric quasi-static simulation code WAKE.<sup>33</sup> A study has been made of plasma densities in the range of  $1.5\text{--}3.5 \times 10^{18} \text{ cm}^{-3}$ , which are comparable with that obtained at the entrance plane in the FLUENT simulation (Fig. 2) and are also typical for LWFA experiments.<sup>8–11</sup> An intense laser pulse propagating through plasma undergoes self-focusing<sup>21</sup> due to the relativistic mass nonlinearity and electron density depletion associated with the ponderomotive pressure.<sup>19</sup> Relativistic effects change the effective dielectric constant of the medium to  $\varepsilon = 1 - \omega_p^2 n_e / (\omega_0^2 \gamma n)$ , where  $\gamma = (1 + a_0^2/2)^{1/2}$  is the Lorentz factor associated with the quiver motion,  $n_e$  is the plasma density, and  $n$  is the unperturbed background plasma density. In our model, we consider the field amplitude of a Gaussian transverse laser pulse profile varying as  $a^2(Z, r) = [a_0^2(Z)/f^2(Z)] \exp[-r^2/w_0^2 f^2(Z)]$ , where  $f(Z) = w(Z)/w_0$  is the normalized pulse radius and  $r$  is the radial coordinate. With the aid of the Poisson equation and at quasi-steady state, we obtain the electron density as a function of the laser vector potential. This density results in the dielectric function  $\varepsilon = \varepsilon_0 - \varepsilon_2 r^2/w_0^2$ , where the second order term  $\varepsilon_2$  is due to the relativistic mass nonlinearity and electron density depletion associated with the ponderomotive pressure of the laser. Following Refs. 34 and 35, we obtain the governing equation for the spot size evolution in a dispersive medium as

$$f''(\xi) - 1/f^3(\xi) + (2\varepsilon_0)^{-1} \varepsilon_0'(\xi) f'(\xi) = (Z_R^2/w_0^2)(\varepsilon_2/\varepsilon_0) f(\xi), \quad (1)$$

where  $\xi = Z/Z_R$ . The second term of (1) is due to diffraction, the third term is due to plasma inhomogeneity and the fourth term is responsible for self-focusing. Equation (1) is a second-order differential equation, which excludes pulse depletion and can be solved upon defining the plasma density profile  $n(Z, r)$  as

$$n(Z, r) = \begin{cases} g(Z)(n_0 + \Delta n r^2/R_1^2) & \text{for } r < R_1, \\ g(Z)(\Delta n + n_0) \frac{r - R_2}{R_1 - R_2} & \text{for } R_1 \leq r \leq R_2, \\ 0 & \text{for } r \geq R_2, \end{cases} \quad (2)$$

where  $g(Z) = (1 + \text{erf}[Z + |L_0|/\delta Z])/2$  describes the plume region,  $L_0 = -3.2 \text{ mm}$  is the initial longitudinal position,  $\delta Z = 3.25 \text{ mm}$  is the density ramp length,  $R_1 = 95 \mu\text{m}$  is the parabolic channel radius,  $R_2 = 150 \mu\text{m}$  is the capillary radius,  $n_0$  is the on-axis density, and  $\Delta n = 0.3n_0$  is the increase in density at  $r = R_1$ . The description of the entrance region density closely matches that inferred from the FLUENT simulation for the electrode geometry. We then apply the boundary condition  $f(-L_0) = w(-L_0)/w_0$  and the initial radius of curvature of the wavefront is equal to the initial curvature in vacuum at  $Z = -L_0$ .

In both the analytic model and the WAKE simulation (Fig. 3), a curved phase-front has been chosen as an initial condition to account for the focusing laser pulse. Focusing in vacuum leads to  $a_0 = 1.0$  at the capillary entrance plane, after which  $a_0$  diminishes as a consequence of diffraction (channel guiding is not included here). Inclusion of plasma in the plume region results in additional self-focusing and, therefore, a higher peak  $a_0$  close to, or at, the entrance plane.

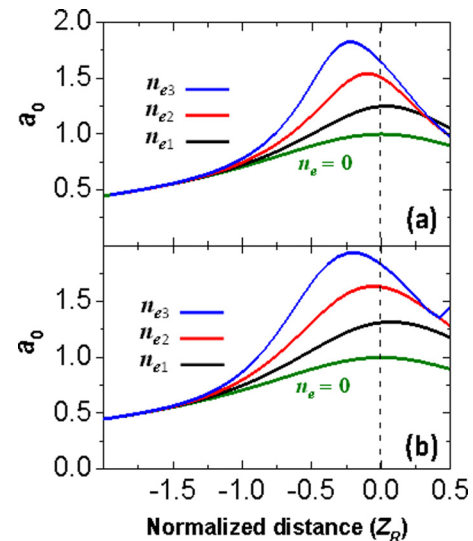


FIG. 3. Laser pulse self-focusing in the plume region showing the evolution of  $a_0$  as a function of the longitudinal distance normalized to the Rayleigh length for density values of  $n_{e1} = 1.54 \times 10^{18} \text{ cm}^{-3}$  (black curves),  $n_{e2} = 2.75 \times 10^{18} \text{ cm}^{-3}$  (red curves), and  $n_{e3} = 3.49 \times 10^{18} \text{ cm}^{-3}$  (blue curves). The vacuum evolution of  $a_0$  is indicated by  $n_e = 0$  (green curves). (a) Analytical solutions and (b) WAKE simulations, where the vertical dashed line marks the entrance plane.

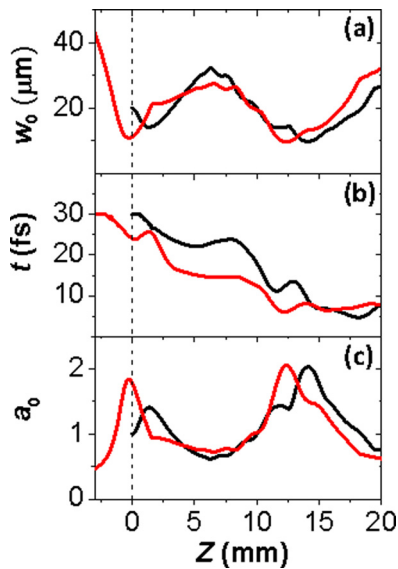


FIG. 4. Evolution of laser pulse (a) width, (b) duration, and (c)  $a_0$  in a plasma channel—WAKE simulations without (black curve) and with (red curve) self-focusing in the plume, where the vertical dashed line marks the entrance plane.

Increasing the density results in stronger self-focusing that can increase  $a_0$  significantly. Similar behaviour is obtained in the two methods and the respective peak  $a_0$  values agree to within 6%. As an example:  $a_0$  reaches 1.83 (analytical) and 1.93 (WAKE) for a density of  $3.49 \times 10^{18} \text{ cm}^{-3}$ . The small discrepancy between the two methods could be due to finite pulse length and pulse depletion effects that are accounted for in the numerical simulations and absent in the analytical calculations. The depletion length  $L_{dep} = \tau c (\omega_0 / \omega_p)^2$ , where  $\tau$  is the pulse duration [see Fig. 4(b) later], in the numerical simulations is appreciably short (only  $\sim 4$  mm at the higher density).

To illustrate the influence of the plasma plume region on the laser pulse evolution in the CDW, WAKE simulations of the waveguide have been carried out both without and with the plume, as shown in Fig. 4, for an on-axis density  $n_e = 3.0 \times 10^{18} \text{ cm}^{-3}$ . In the former case, the laser is focused in vacuum onto the entrance plane [peak  $a_0 = 1.0$ ], while for the latter case, self-focusing in the plume is included, as in Fig. 3(b) [peak  $a_0 \approx 1.8$ ]. Both cases show that variation of the spot size due to self-focusing leads to a mismatch of the waveguide and high order transverse modes are excited, which result in scalloping. The matched waist  $R_m [\mu\text{m}] \approx 1.48 \times 10^5 R_w^{1/2} [\mu\text{m}] / n_e^{1/4} [\text{cm}^{-3}] = 36 \mu\text{m}$ , for a  $R_w \approx 100 \mu\text{m}$  parabolic channel radius<sup>16</sup> is larger than the self-focused waist and results in peaks in  $a_0$  separated by a period  $\approx 12$  mm (close to the low intensity scallop period

$\lambda_C = \pi^2 R_m^2 / \lambda = 16$  mm). In both cases (with and without plume),  $a_0 \approx 2.0$  after one scallop period. However, the evolution of  $a_0$  around the capillary entrance is very different.

Without the plume  $a_0$  increases from 1.0 to only 1.41 at  $Z = 1.4$  mm, while inclusion of the plume leads to  $a_0 = 1.85$  at  $Z = -0.3$  mm, a 30% increase, which corresponds to a 70% increase in the intensity. As shown in Fig. 5, this drives a strongly non-linear plasma wakefield at the beginning of the waveguide. The initial growth of  $a_0$  arises primarily from the laser waist size reduction [Fig. 4(a)] with subsequent pulse length compression [Fig. 4(b)] and photon deceleration contributing significantly to the growth of  $a_0$  at one scallop period. This later growth in  $a_0$  is driven by the spatio-temporal density profile of the wakefield bubble. In the LWFA, the position along the capillary where electron self-injection occurs and acceleration begins will depend on particular experimental parameters but our results show that the laser evolution in the plume region may, in many cases, lead to self-injection within the first mm of the waveguide. This subject will be discussed elsewhere.

#### IV. EXPERIMENTAL PLUME MEASUREMENTS

To investigate the case, where a very long plasma plume is ejected following the generation and expansion of the hot plasma, we have carried out time-averaged measurements (Fig. 6) by imaging fluorescence from the plume in the transverse plane onto either a charge-coupled device (CCD) camera (pixel size  $4.65 \mu\text{m}$ ), to obtain a 2D image, or onto the narrow entrance slit (width  $10 \mu\text{m}$ ) of an imaging optical spectrometer (resolution  $1.4 \text{ nm}$ ) to measure the spectra of Stark-broadened hydrogen Balmer line emission<sup>36</sup> from the background gas neutral atoms. The latter method enables the spatially resolved electron plasma density to be measured. Self-absorption leads to an over-estimation of the absolute density<sup>37</sup> compared with interferometry techniques.<sup>32</sup> The longitudinal variation of the fluorescence has been studied at intervals of  $0.5$  mm by translating the relay lens and detectors together, where the step size is chosen to be larger than the depth-of-focus ( $\sim 0.1$  mm). Measurements are time-averaged because a  $2$  ms shutter opening time has been used for both diagnostic methods employed here (CCD imaging and Stark spectroscopy). However, the peak density is approximately double the time-averaged value.<sup>38</sup> Furthermore, the similarity between the transverse profiles of CCD and the spectral data, as illustrated in Fig. 7, show that the CCD images can be used as a reliable qualitative measurement of plasma density variations. Both of our diagnostic methods resolve the characteristic parabolic profile of the channel.<sup>16</sup>

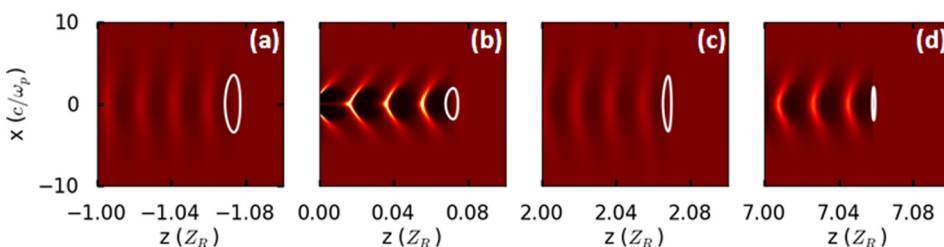


FIG. 5. WAKE simulations of the plasma channel including plume, which show four profiles of the plasma density wakefield at distance  $Z =$  (a)  $-1.7$  mm, (b)  $0.1$  mm, (c)  $3.2$  mm, and (d)  $11.1$  mm. The white contour indicates the position of the laser pulse and its iso-intensity (at half-height).

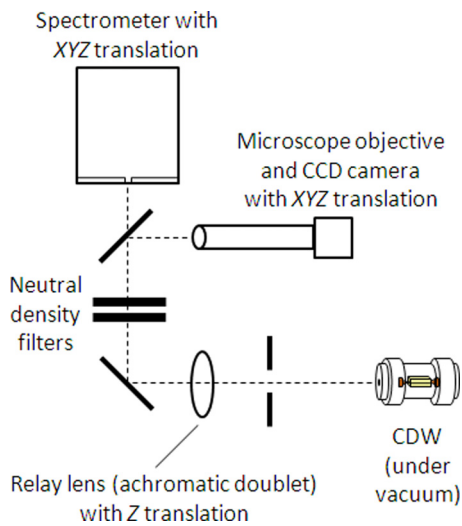


FIG. 6. Experimental setup for characterizing the plume fluorescence. The CDW is located in a vacuum chamber and a translatable  $2f$  image relay, where  $f=300$  mm is the lens focal length, is used to image the transverse focal plane as a function of position.

The on-axis density of this plasma plume in the 3 mm region of interest is found to be almost equal to that inside the capillary. Figure 8 compares two transverse density profiles obtained by measuring Stark-broadening using the spectrometer. The parabola formed inside the capillary quickly flattens at  $\approx 1$  mm resulting in a uniform transverse profile and remains flat until  $Z=-3$  mm and beyond. Only beyond  $Z=-3$  mm does the on-axis density begin to decrease slightly, as shown in the CCD camera data of Fig. 9. Light scattered off the inner surface of the electrode aperture [Fig. 9(a)] highlights the electrode edge and helps to illustrate the tight confinement of the plume even up to  $Z=-8$  mm (i.e., that a “plasma plume jet” is formed). These measurements show that the on-axis plasma density remains high, in contrast to the steady-state FLUENT simulations of neutral cold gas that show a density decrease around the entrance ( $Z=0$  mm) and between the inlet and the entrance ( $Z=10$  mm).

Our measurements show that the on-axis density does not decrease by an order of magnitude until  $Z=-30$  mm, i.e., beyond the Perspex housing, and a linear drop-off is

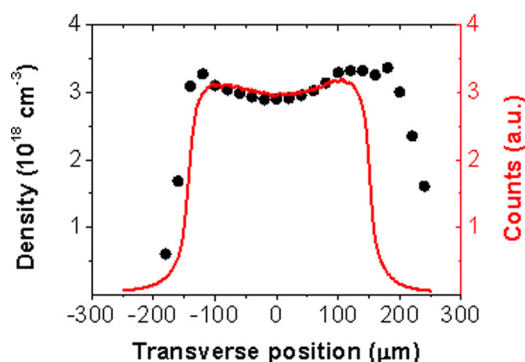


FIG. 7. Transverse profile of the Stark-broadening derived plasma density (closed circles) and CCD camera image (red curve), where zero transverse position denotes the centre of the capillary. Backing pressure is  $(115 \pm 5)$  mbar and  $Z=0$  mm.

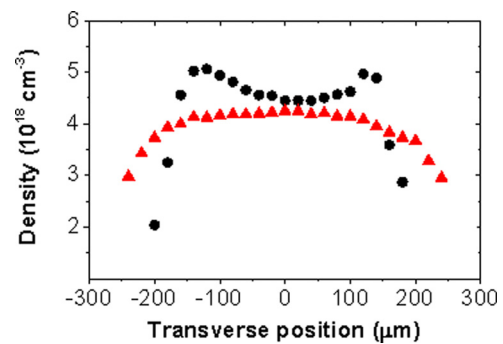


FIG. 8. Transverse profile of the Stark-broadening-derived plasma density inside the capillary ( $Z=3$  mm; black circles) and outside the capillary ( $Z=-3$  mm; red triangles), where zero transverse position denotes the centre of the capillary. Backing pressure is  $(165 \pm 5)$  mbar.

maintained up to  $Z=-60$  mm. A weak dependence on the gas backing pressure (in the range of 40–160 mbar) has been found for the density drop-off. Reduced gas flow at lower pressure reduces the pressure of the expanding plume (the plasma temperature is also lower<sup>16</sup>), marginally increasing the rate of density drop-off. However, the relative difference is negligible in the region of interest up to  $Z=-3$  mm. At any given pressure, therefore, the on-axis density along the region of interest can be taken to be constant, to within experimental uncertainty. The steady-state neutral gas simulations (Fig. 2) predict a much more rapid drop-off of the density than that measured experimentally. It is therefore concluded that the steady-state simulations exaggerate the role of the electrode geometry. The measurements show that the electrode/housing regions have negligible influence on the on-axis density and hence self-focusing in the plume must always be accounted for. This would apply even for very short electrode/housing regions.

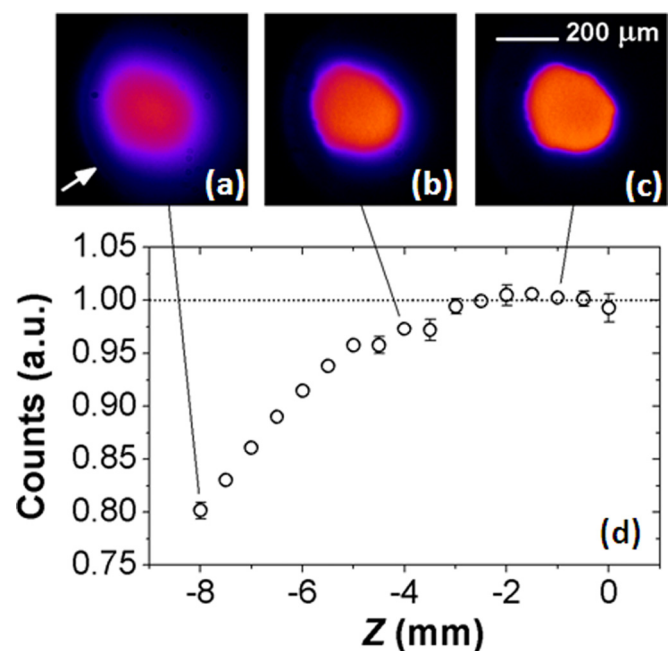


FIG. 9. (a)–(c) Three false colour camera images, where the arrow in (a) indicates the edge of the electrode aperture and (d) relative CCD camera intensity of the central portion of the plume as a function of distance in front of the capillary entrance plane. Backing pressure is  $(165 \pm 5)$  mbar.

Consideration must now be given to how these time-averaged measurements apply to gas-filled CDW laser wake-field experiments. Gas pre-injection on the ms timescale ensures that the neutral gas plume is always extremely long and of high density, however, the precise extent of the expanding plasma plume as encountered by the incident laser pulse is specific to each experiment. The density profile of the plasma plume drops off exponentially away from the capillary entrance with a leading edge velocity (at  $n_e/e$ ) of  $\sim 1 \times 10^4$  m/s.<sup>28</sup> Establishing a parabolic channel can take as little as 50 ns after the onset of the discharge<sup>16</sup> however electron injection typically occurs after a further  $\sim 100$  ns<sup>8–10,17</sup> such that the plasma plume leading edge has propagated  $\sim 2$  mm upon laser arrival. The time-averaged measurements would, in such a case, overestimate the plasma plume density in the region of interest and laser self-ionization of the neutral gas would be required to drive the strong self-focusing, most of which is predicted to occur within one just Rayleigh length of the capillary entrance (Fig. 3). A denser expanding plasma plume in the region of interest requires a larger discharge/laser delay time and/or a hotter, more rapidly expanding plume. Clearly, a time-resolved study of the expanding plasma plume on the sub-microsecond timescale would be of interest although it must be reiterated that the long neutral gas plume would support the requisite laser self-ionization.

## V. SUMMARY

It is shown that the gas/plasma plume of a CDW can have an on-axis density that is comparable with that in the capillary for a significant distance beyond its entrance (and exit) plane, and therefore must be taken into account for high-intensity laser pulses, where self-ionization of the gas plume and subsequent self-focusing leads to a rapid increase in intensity and a plasma density wake. Self-focusing in the plume leads to an increase in  $a_0$  at the beginning of the waveguide, which may lead to early electron injection and acceleration, in contrast with middle-to-late<sup>9</sup> injection and acceleration. This has implications for the length of capillary required for electron beam generation, and also for the position of the focus of the laser beam. It is well known that the capillary length must exceed the dephasing length, where electrons outrun the plasma wave, and, thus, has a bearing on the electron beam parameters including beam quality.<sup>6</sup> The scallop period  $\lambda_C$  scales inversely with  $n_e$ . However, if injection is guaranteed to occur early, the required length would only be of the order of 3–8 mm for our parameters. Shorter CDWs would have the advantage in that lower discharge voltages are sufficient for breakdown, and laser beam alignment is easier because the capillary is only two or three Rayleigh lengths long and much shorter than  $\lambda_C$ .

The extent of the plume to be considered depends on the laser parameters and focusing conditions. For example, matching to the capillary studied here ( $n_e = 3.0 \times 10^{18}$  cm<sup>-3</sup>,  $R_m = 36$   $\mu$ m) considerably lengthens the Rayleigh length ( $Z_R \approx 5$  mm in this case compared with 1.6 mm considered above). The larger  $F$ /number will lead to earlier self-focusing if the laser power is sufficient and, therefore, a longer plume region will need to be considered. Given that the

on-axis plume density decreases with distance beyond  $-3$  mm, the longitudinal variation in density must be properly described and, hence, the specific geometric design of the capillary electrode/housing will become important if the radially expanding plasma plume jet impinges on it.

## ACKNOWLEDGMENTS

We acknowledge support of the U.K. EPSRC, the EC's LASERLAB-EUROPE/LAPTECH (Grant Agreement No. 284464), EuCARD-2 (Grant Agreement No. 312453), and the Extreme Light Infrastructure (ELI) European Project. We thank S. Kalmykov and N. Bourgeois for discussions on WAKE and D. Clark and T. McCann for technical support.

<sup>1</sup>D. J. Spence and S. M. Hooker, *Phys. Rev. E* **63**, 015401 (2000).

<sup>2</sup>T. Tajima and J. M. Dawson, *Phys. Rev. Lett.* **43**, 267 (1979).

<sup>3</sup>S. P. D. Mangles, C. D. Murphy, Z. Najmudin, A. G. R. Thomas, J. L. Collier, A. E. Dangor, E. J. Divall, P. S. Foster, J. G. Gallacher, C. J. Hooker, D. A. Jaroszynski, A. J. Langley, W. B. Mori, P. A. Norreys, F. S. Tsung, R. Viskup, B. R. Walton, and K. Krushelnick, *Nature (London)* **431**, 535 (2004).

<sup>4</sup>C. G. R. Geddes, C. Toth, J. van Tilborg, E. Esarey, C. B. Schroeder, D. Bruhwiler, C. Nieter, J. Cary, and W. P. Leemans, *Nature (London)* **431**, 538 (2004).

<sup>5</sup>J. Faure, Y. Glinec, A. Pukhov, S. Kiselev, S. Gordienko, E. Lefebvre, J.-P. Rousseau, F. Burgy, and V. Malka, *Nature (London)* **431**, 541 (2004).

<sup>6</sup>E. Esarey, C. B. Schroeder, and W. P. Leemans, *Rev. Mod. Phys.* **81**, 1229 (2009).

<sup>7</sup>S. M. Wiggins, R. C. Issac, G. H. Welsh, E. Brunetti, R. P. Shanks, M. P. Anania, S. Cipiccia, G. G. Manahan, C. Aniculaesei, B. Ersfeld, M. R. Islam, R. T. L. Burgess, G. Vieux, W. A. Gillespie, A. M. MacLeod, S. B. van der Geer, M. J. de Loos, and D. A. Jaroszynski, *Plasma Phys. Controlled Fusion* **52**, 124032 (2010).

<sup>8</sup>S. Karsch, J. Osterhoff, A. Popp, T. P. Rowlands-Rees, Z. Major, M. Fuchs, B. Marx, R. Hörlein, K. Schmid, L. Veisz, S. Becker, U. Schramm, B. Hidding, G. Pretzler, D. Habs, F. Grüner, F. Krausz, and S. M. Hooker, *New J. Phys.* **9**, 415 (2007).

<sup>9</sup>T. P. A. Ibbotson, N. Bourgeois, T. P. Rowlands-Rees, L. S. Caballero, S. I. Bajilekov, P. A. Walker, S. Kneip, S. P. D. Mangles, S. R. Nagel, C. A. J. Palmer, N. Delerue, G. Doucas, D. Urner, O. Chekhlov, R. J. Clarke, E. Divall, K. Ertel, P. Foster, S. J. Hawkes, C. J. Hooker, B. Parry, P. P. Rajeev, M. J. V. Streeter, and S. M. Hooker, *New J. Phys.* **12**, 045008 (2010).

<sup>10</sup>S. Cipiccia, M. R. Islam, B. Ersfeld, R. P. Shanks, E. Brunetti, G. Vieux, X. Yang, R. C. Issac, S. M. Wiggins, G. H. Welsh, M. P. Anania, D. Maneuski, R. Montgomery, G. Smith, M. Hoek, D. J. Hamilton, N. R. C. Lemos, R. A. Bendoyro, D. Symes, P. P. Rajeev, V. O'Shea, J. M. Dias, and D. A. Jaroszynski, *Nature Phys.* **7**, 867 (2011).

<sup>11</sup>W. P. Leemans, B. Nagler, A. J. Gonsalves, C. Toth, K. Nakamura, C. G. R. Geddes, E. Esarey, C. B. Schroeder, and S. M. Hooker, *Nature Phys.* **2**, 696 (2006).

<sup>12</sup>V. M. Malkin, G. Shvets, and N. J. Fisch, *Phys. Rev. Lett.* **82**, 4448 (1999).

<sup>13</sup>G. Vieux, A. Lyachev, X. Yang, B. Ersfeld, J. P. Farmer, E. Brunetti, R. C. Issac, G. Raj, G. H. Welsh, S. M. Wiggins, and D. A. Jaroszynski, *New J. Phys.* **13**, 063042 (2011).

<sup>14</sup>R. M. G. M. Trines, F. Fiuza, R. Bingham, R. A. Fonseca, L. O. Silva, R. A. Cairns, and P. A. Norreys, *Phys. Rev. Lett.* **107**, 105002 (2011).

<sup>15</sup>V. Malka, *Phys. Plasmas* **19**, 055501 (2012).

<sup>16</sup>N. A. Brobova, A. A. Esaulov, J.-I. Sakai, P. V. Sasorov, D. J. Spence, A. Butler, S. M. Hooker, and S. V. Bulanov, *Phys. Rev. E* **65**, 016407 (2001).

<sup>17</sup>T. P. Rowlands-Rees, C. Kamperidis, S. Kneip, A. J. Gonsalves, S. P. D. Mangles, J. G. Gallacher, E. Brunetti, T. Ibbotson, C. D. Murphy, P. S. Foster, M. J. V. Streeter, F. Budde, P. A. Norreys, D. A. Jaroszynski, K. Krushelnick, Z. Najmudin, and S. M. Hooker, *Phys. Rev. Lett.* **100**, 105005 (2008).

<sup>18</sup>E. Esarey, P. Sprangle, and J. Krall, *IEEE J. Quantum Electron.* **33**, 1879 (1997).

<sup>19</sup>H. Hora, *Z. Phys.* **226**, 156 (1969).



- <sup>20</sup>A. Pukhov and J. Meyer-ter-Vehn, *Appl. Phys. B* **74**, 355 (2002).
- <sup>21</sup>P. Sprangle, C. M. Tang, and E. Esarey, *IEEE Trans. Plasma Sci.* **15**, 145 (1987).
- <sup>22</sup>W. Lu, M. Tzoufras, C. Joshi, F. S. Tsung, W. B. Mori, J. Vieira, R. A. Fonseca, and L. O. Silva, *Phys. Rev. ST Accel. Beams* **10**, 061301 (2007).
- <sup>23</sup>L. S. Caballero, H. Chuaqui, M. Favre, I. Mitchell, and E. Wyndham, *J. Appl. Phys.* **98**, 023305 (2005).
- <sup>24</sup>J. Kędzierski, J. Engemann, M. Teschke, and D. Korzec, *Solid State Phenom.* **107**, 119 (2005).
- <sup>25</sup>X. Wang, G. Wang, Z. Ma, K. Dong, B. Zhu, Y. Wu, and Y. Gu, *J. Plasma Phys.* **78**, 483 (2012).
- <sup>26</sup>S. M. Wiggins, M. P. Reijnders, S. Abuazoum, K. Hart, G. H. Welsh, R. C. Issac, D. R. Jones, and D. A. Jaroszynski, *Rev. Sci. Instrum.* **82**, 096104 (2011).
- <sup>27</sup>S. Abuazoum, S. M. Wiggins, R. C. Issac, G. H. Welsh, G. Vieux, M. Ganciu, and D. A. Jaroszynski, *Rev. Sci. Instrum.* **82**, 063505 (2011).
- <sup>28</sup>J. Denavit, *Phys. Fluids* **22**, 1384 (1979).
- <sup>29</sup>D. Kaganovich, P. V. Satorov, Y. Ehrlich, C. Cohen, and A. Zigler, *Appl. Phys. Lett.* **71**, 2925 (1997).
- <sup>30</sup>D. A. Jaroszynski, R. Bingham, E. Brunetti, B. Ersfeld, J. Gallacher, B. van der Geer, R. Issac, S. P. Jamison, D. Jones, M. de Loos, A. Lyachev, V. Pavlov, A. Reitsma, Y. Saveliev, G. Vieux, and S. M. Wiggins, *Philos. Trans. R. Soc. London, Ser. A* **364**, 689 (2006).
- <sup>31</sup>Fluent Inc., *FLUENT User's Guide* (Fluent Inc., Lebanon, NH, 2003).
- <sup>32</sup>A. J. Gonsalves, T. P. Rowlands-Rees, B. H. P. Broks, J. J. A. M. van der Mullen, and S. M. Hooker, *Phys. Rev. Lett.* **98**, 025002 (2007).
- <sup>33</sup>P. Mora and T. M. Antonsen, Jr., *Phys. Plasmas* **4**, 217 (1997).
- <sup>34</sup>S. A. Akhmanov, A. P. Sukhorukov, and R. V. Khokhlov, *Sov. Phys. Usp.* **10**, 609 (1968).
- <sup>35</sup>C. S. Liu and V. K. Tripathi, *Interaction of Electromagnetic Waves with Electron Beams and Plasmas* (World Scientific, Singapore, 1994), p. 119.
- <sup>36</sup>J. Ashkenazy, R. Kipper, and M. Caner, *Phys. Rev. A* **43**, 5568 (1991).
- <sup>37</sup>D. G. Jang, M. S. Kim, I. H. Nam, H. S. Uhm, and H. Suk, *Appl. Phys. Lett.* **99**, 141502 (2011).
- <sup>38</sup>S. Abuazoum, S. M. Wiggins, B. Ersfeld, K. Hart, G. Vieux, X. Yang, G. H. Welsh, R. C. Issac, M. P. Reijnders, D. R. Jones, and D. A. Jaroszynski, *Appl. Phys. Lett.* **100**, 014106 (2012).